Chapter 4

RADIATIVE PROPERTIES OF (SPHERICAL) PARTICLES AND OF PARTICLE-SIZE DISTRIBUTIONS*

Extinction of radiation by spherical (conducting or nonconducting) particles is conventionally treated theoretically by following the classical analysis of Mie.[1–5,†] The limiting cases for particles that are either small or large compared with the wavelength of light are, however, more easily derived by following the older treatments of Rayleigh and of Kirchhoff and Huygens. A complete derivation of the equations summarized in the following Section 4-1 may be found in Stratton[2] and other authoritative treatises.[3–5]

4-1 Diffraction of a plane wave by a spherical particle

Mie considered a sphere of radius r and propagation constant $k_s = 2\pi/\lambda_s$ (where λ_s is the wavelength of light in the sphere) embedded in an infinite, non-conducting medium with propagation constant $k_m = 2\pi/\lambda_m$ (λ_m = wavelength of light in the medium). For an incident plane wave, polarized in the x-direction and propagating in the z-direction, it may then be shown[1,2] that the following relations apply:

$$\text{mean energy flow of the incident wave per unit area} = \bar{S}_z = \frac{1}{2} E_0^2 \left(\frac{\epsilon_m}{\mu_m}\right)^{1/2}, \tag{4-1.1}$$

* Chapter 4 is by S. S. Penner.

† The author is indebted to Dr. G. N. Plass for some helpful comments. For recently published survey papers on Mie scattering and absorption cross sections for absorbing particles, see Plass.[5a]

where E_0 is the amplitude of the incident electric field and ϵ_m and μ_m represent, respectively, the permittivity and permeability of the infinite medium;

$$\text{scattered energy} = W_s = \pi \frac{E_0^2}{k_m^2} \left(\frac{\epsilon_m}{\mu_m}\right)^{1/2} \sum_{n=1}^{\infty} (2n+1)\,(|\,a_n^r\,|^2 + |\,b_n^r\,|^2), \tag{4-1.2}$$

where

$$a_n^r = -\frac{\mu_s j_n(N\rho)\,[\rho j_n(\rho)]' - \mu_m j_n(\rho)\,[N\rho j_n(N\rho)]'}{\mu_s j_n(N\rho)\,[\rho h_n^{(1)}(\rho)]' - \mu_m h_n^{(1)}(\rho)\,[N\rho j_n(N\rho)]'}, \tag{4-1.3}$$

$$b_n^r = -\frac{\mu_s j_n(\rho)\,[N\rho j_n(N\rho)]' - \mu_m N^2 j_n(N\rho)\,[\rho j_n(\rho)]'}{\mu_s h_n^{(1)}(\rho)\,[N\rho j_n(N\rho)]' - \mu_m N^2 j_n(N\rho)\,[\rho h_n^{(1)}(\rho)]'}, \tag{4-1.4}$$

$\rho = k_m r$; N = complex index of refraction of the sphere relative to the ambient medium $\equiv N_1 + iN_2$; $j_n(x) = (\pi/2x)^{1/2} J_{n+\frac{1}{2}}(x)$, where $J_m(x)$ is the Bessel function of order m; $h_n^{(1)}(x) = (\pi/2x)^{1/2} H_{n+\frac{1}{2}}^{(1)}(x)$, where $H_m^{(1)}(x) = J_m(x) + iN_m(x)$ is a Hankel function and $N_m(x)$ is a Bessel function of the second kind;

$$\text{sum of absorbed and scattered energy} = W_t = \pi \frac{E_0^2}{k_m^2} \left(\frac{\epsilon_m}{\mu_m}\right)^{1/2} \text{Re}\left\{\sum_{n=1}^{\infty} (2n+1)\,(a_n^r + b_n^r)\right\}; \tag{4-1.5}$$

$$\text{scattering cross section} = Q_s = \frac{W_s}{S_z} = \frac{2\pi}{k_m^2}\left\{\sum_{n=1}^{\infty} (2n+1)\,(|\,a_n^r\,|^2 + |\,b_n^r\,|^2)\right\}; \tag{4-1.6}$$

$$\text{scattering coefficient or scattering efficiency factor} = \frac{Q_s}{\pi r^2}; \tag{4-1.7}$$

$$\text{total cross section} = Q_t = \frac{W_t}{S_z} = \frac{2\pi}{k_m^2} \text{Re}\left\{\sum_{n=1}^{\infty} (2n+1)\,(a_n^r + b_n^r)\right\}; \tag{4-1.8}$$

$$\text{efficiency factor for extinction} = \frac{Q_t}{\pi r^2}; \tag{4-1.9}$$

$$\text{absorption efficiency factor} = \frac{(Q_t - Q_s)}{\pi r^2}. \tag{4-1.10}$$

Equations (4-1.2) to (4-1.10) contain the complete results of the Mie theory and have been used in recent electronic computer programs on carbon[6] and on aluminum or magnesium oxide.[7,7a]

Quantitative calculations according to the Mie theory require knowledge of particle radius, wavelength, and the complex index of refraction $N \equiv N_1 + iN_2$ of the spheres. Methods for the direct or indirect determination of N are discussed in the literature.[3,6,7,7a] The real part N_1 is believed to vary slowly with temperature, although experimental data at temperatures other than room temperature are so limited that this hypothesis cannot be considered to have been proved experimentally.[7,7a] For (polycrystalline) aluminum oxide, Plass[7] used sapphire values and stated that the interaction between an electromagnetic wave and a small particle ($r < \lambda_s$) is essentially the same for a single crystal and a polycrystalline particle. Efficiency factors have been calculated for Al_2O_3 and MgO with particle radii of 0.1 to 10 μ and $0.5 \leqslant \lambda_m(\mu) \leqslant 10$;[7,7a] representative smoothed plots through the calculated points are reproduced in Figs. 4-1.1 through 4-1.4. Total and scattering cross sections have been calculated for carbon particles with radii between 47.8 and

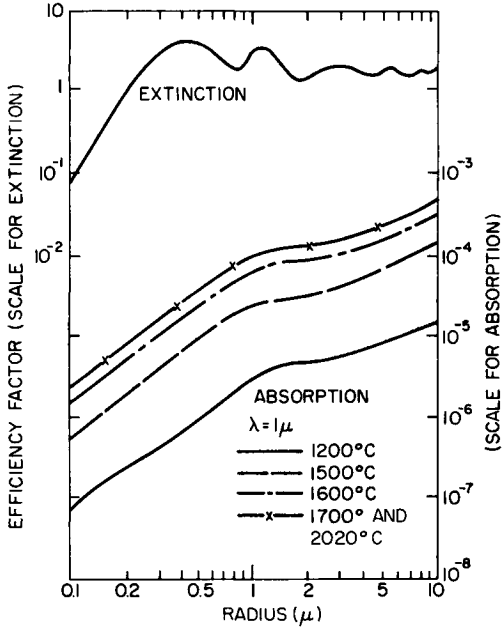

FIG. 4-1.1. Efficiency factor (cross section divided by cross-sectional area of particle) for Al_2O_3 as a function of particle radius at a wavelength of 1 μ. The upper curve gives the efficiency factor for extinction at all temperatures from 1200 to 2020°C. The lower curves give the efficiency factors for absorption at various temperatures from 1200 to 2020°C. The curves for 1700 and 2020°C coincide on this scale. Note the different scales for extinction and absorption. Reproduced from Plass.[7a]

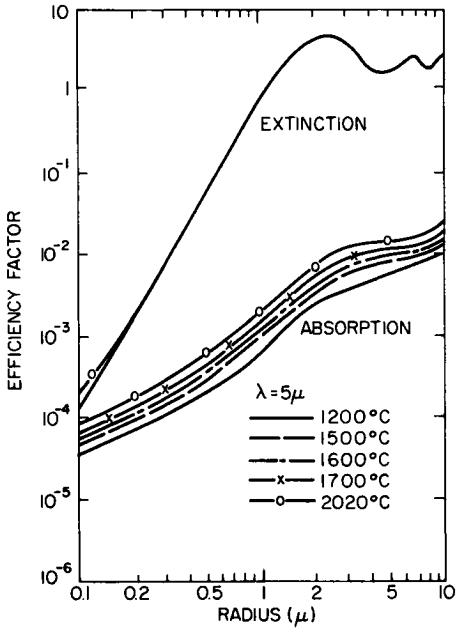

FIG. 4-1.2. Efficiency factor for Al_2O_3 as a function of particle radius at a wavelength of 5μ. The upper curves give the efficiency factors for extinction at 1200 and 2020°C. The lower curves give the efficiency factors for absorption at various temperatures. Reproduced from Plass.[7a]

987 Å for $1 \leqslant \lambda_m(\mu) \leqslant 20$; representative results are reproduced in Figs. 4-1.5 and 4-1.6.

The following limiting cases may be derived from the general relations (see Section 4-2) and are seen to be verified by the data plotted in Figs. 4-1.1 to 4-1.4: (a) for $r \ll \lambda$, $(Q_t - Q_s)/\pi r^2 \equiv Q_a/\pi r^2$ is proportional to r, and $Q_s/\pi r^2$ is proportional to r^4; (b) for $r \gg \lambda$, Q_t approaches $2\pi r^2$, i.e., the efficiency factor for extinction $(= Q_t/\pi r^2)$ approaches the value 2.

Unless r is several orders of magnitude smaller than λ_m, Q_s is much larger than the absorption cross section $Q_t - Q_s$ because the absorption coefficient is very small for Al_2O_3 and MgO in the wavelength range considered. Thus $Q_t/Q_s \simeq 1.000$ for both Al_2O_3 and MgO, $\lambda_m = 2\,\mu$, and $0.1 \leqslant r(\mu) \leqslant 9.9$; also $Q_t/Q_s \simeq 1.000$ for both Al_2O_3 and MgO, $\lambda_m = 5\,\mu$, and $0.8 \leqslant r(\mu) \leqslant 9.9$. However, for $\lambda_m = 5\,\mu$ and $r \leqslant 0.6\,\mu$, the data listed in Table 4-1.1 apply.

The computer output data contain information on the angular distribution of the scattered radiation. For $r \ll \lambda$, the ratio of forward

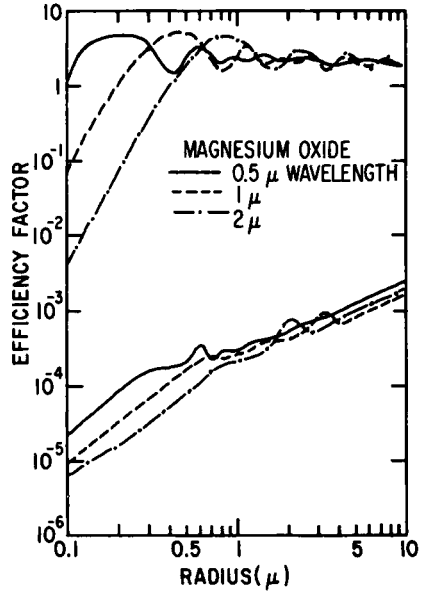

FIG. 4-1.3. Efficiency factor for MgO as a function of particle radius at wavelengths of 0.5, 1, and 2 μ. The upper curves give the efficiency factor for extinction, while the lower curves give the efficiency factor for absorption. Reproduced from Plass.[7]

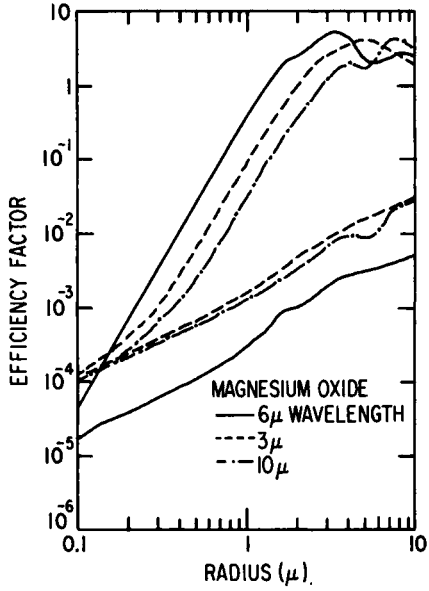

FIG. 4-1.4. Efficiency factor for MgO as a function of particle radius at wavelengths of 6, 8, and 10 μ. The upper curves give the efficiency factor for extinction, while the lower curves give the efficiency factor for absorption. Reproduced from Plass.[7]

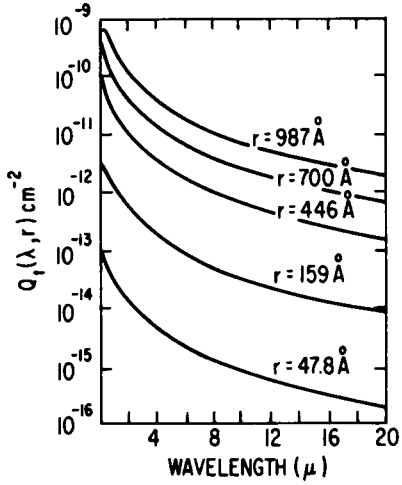

FIG. 4-1.5. Total cross section Q_t as a function of wavelength for carbon particles of various radii; reproduced from Stull and Plass.[6]

to backward scattering becomes equal to unity; for $r \gg \lambda$, preferential scattering occurs in the forward direction (see Section 4-2 for a discussion of limiting cases). Representative results on the ratio of forward to backward scattering intensities, and on the angular distribution of the scattered intensity, are summarized in Figs. 4-1.7 and 4-1.8.

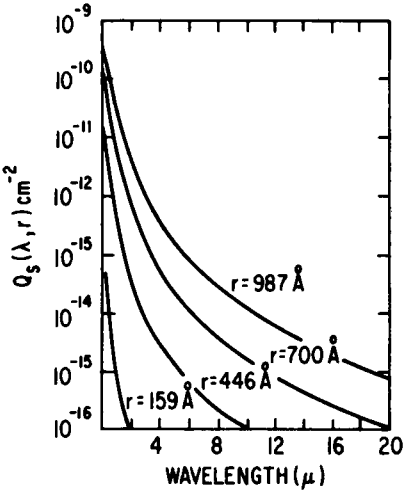

FIG. 4-1.6. Scattering cross section Q_s as a function of wavelength for carbon particles of various radii; reproduced from Stull and Plass.[6]

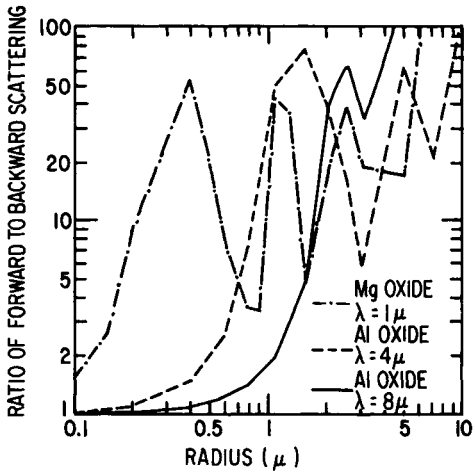

FIG. 4-1.7. Ratio of forward ($\theta = 0°$) to backward ($\theta = 180°$) scattering as a function of particle size for MgO at a wavelength of 1 μ and for Al_2O_3 at wavelengths of 4 and 8 μ. Reproduced from Plass.[7]

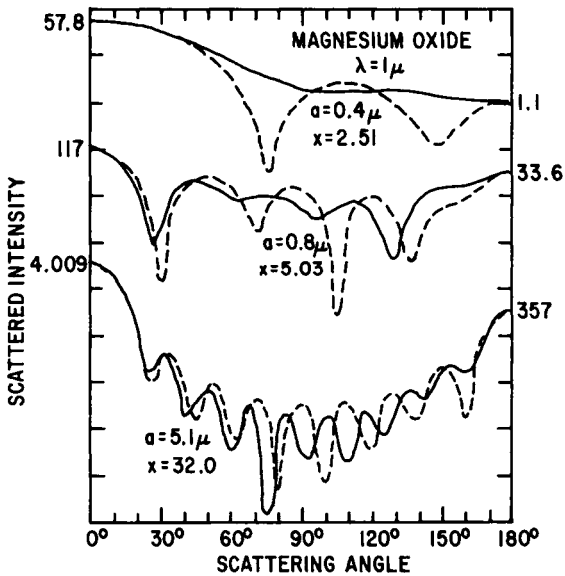

FIG. 4-1.8. Scattered intensity as a function of scattering angle for MgO at a wavelength of 1 μ. The dotted curve is the intensity i_1 and the solid curve is the intensity i_2 (as defined by Van de Hulst[5]). In all graphs, the logarithm of the intensity (each division is a factor of 10) is plotted against the scattering angle (each division is 30°). The values for 0° and 180° are indicated in the margins. The values were calculated at 5° intervals. The quantity x is equal to $2\pi a/\lambda$, where a is the radius of the particle and λ is the wavelength. Reproduced from Plass.[7]

TABLE 4-1.1

REPRESENTATIVE VALUES OF Q_t/Q_s FOR Al_2O_3 AND MgO, CALCULATED FROM THE DATA IN PLASS[7]

λ_m , μ	r, μ	$(Q_t/Q_s)_{Al_2O_3}$	$(Q_t/Q_s)_{MgO}$
5	0.1	1.257	1.124
	0.2	1.034	1.016
	0.4	1.004	1.004
	0.6	1.000	1.000

4-2 Limiting cases of the Mie theory for scattering by spherical particles

The general relations summarized in Eqs. (4-1.2) to (4-1.10) are so complex that machine computations are required for proper evaluation of results, as has been discussed in Section 4-1. However, when r is either small or large compared to λ, then relatively simple asymptotic results may be derived. These limiting cases will now be considered briefly.

4-2A RAYLEIGH SCATTERING ($|\rho| \ll 1$). The parameter

$$\rho = k_m r = 2\pi r/\lambda_m$$

measures essentially the ratio of the particle radius to the wavelength of the radiation in the ambient medium. For $\rho \ll 1$, such that powers of ρ larger than ρ^5 may be neglected, it may be shown[2] that

$$a_1^r \simeq \frac{i}{3}\frac{2\rho^3}{\mu_s + 2\mu_m}\left\{\mu_s - \mu_m - \frac{1}{10}[\mu_s(2 + N^2) - \mu_m(1 + 2N^2)]\,\rho^2\right\}$$

or

$$a_1^r \simeq \frac{i}{45}(N^2 - 1)\,\rho^5 \qquad \text{for} \quad \mu_s = \mu_m\,; \tag{4-2.1}$$

$$a_2^r \simeq \frac{i}{15}\frac{\mu_s - \mu_m}{2\mu_s + 3\mu_m}\rho^5$$

or

$$a_2^r = 0 \qquad \text{for} \quad \mu_s = \mu_m\,; \tag{4-2.2}$$

$$b_1^r \simeq -\frac{2i}{3}\frac{\rho^3}{2\mu_s+\mu_m N^2}\left\{\mu_s-\mu_m N^2-\frac{1}{10}[\mu_s(1+2N^2)-\mu_m N^2(2+N^2)]\,\rho^2\right\}$$

or

$$b_1^r \simeq +\frac{2i}{3}\left(\frac{N^2-1}{N^2+2}\rho^3-\frac{1}{10}\frac{N^4-1}{N^2+2}\rho^5\right) \qquad \text{for} \qquad \mu_s=\mu_m\,; \tag{4-2.3}$$

$$b_2^r \simeq -\frac{i}{15}\frac{\mu_s-\mu_m N^2}{3\mu_s+2\mu_m N^2}\rho^5$$

or

$$b_2^r \simeq +\frac{i}{15}\frac{N^2-1}{2N^2+3}\rho^5 \qquad \text{for} \quad \mu_s=\mu_m\,. \tag{4-2.4}$$

For $\mu_s=\mu_m$, it is now readily seen that the scattering efficiency factor, including terms up to ρ^4, becomes

$$\kappa_s \equiv \frac{Q_s}{\pi r^2} \simeq \frac{8}{3}\left(\frac{N^2-1}{N^2+2}\right)^2\rho^4 = \frac{128}{3}\left(\frac{\pi r}{\lambda}\right)^4\left(\frac{N^2-1}{N^2+2}\right)^2, \tag{4-2.5}$$

where the next higher-order term is easily evaluated and is proportional to ρ^6. Equation (4-2.5) is Rayleigh's expression for the scattering coefficient κ_s. The amplitude $b_1^r = -(2i/3)(N^2-1)\,\rho^3/(N^2+2)$ corresponds to a field, the fundamental mode of which is that of an electric dipole along the x-axis with moment $4\pi\epsilon_m(N^2-1)\,r^3E_0/(N^2+2)$.[2]

Equation (4-2.5) does not contain the angular dependence of the scattered intensity. For Rayleigh scattering, it may be shown[4] that the angular distribution is determined by the factor

$$\frac{P'(\cos\theta)}{4\pi} = \frac{3}{16\pi}(1+\cos^2\theta) \qquad \text{for unpolarized light,}$$

where θ is the angle between the direction of propagation of radiation and the direction of observation used. The function $P'(\cos\theta)/4\pi$ is normalized in such a way that its integral over the complete solid angle Ω is unity, i.e.,

$$\kappa_s(\theta) = \frac{3}{16\pi}(1+\cos^2\theta)\,\kappa_s\,, \tag{4-2.5a}$$

where

$$\int \kappa_s(\theta)\,d\Omega = \kappa_s\,.$$

Furthermore, since $[\cos^2(\pi-\theta)] = \cos^2\theta$, it follows that the ratio of forward to backward scattering is unity in the Rayleigh limit.

Scattering cross sections may be predicted, in fair approximation, by using a step function in which the Rayleigh limit is used for $Q_s/\pi r^2 < 2$ and the Kirchhoff-Huygens limit $Q_s/\pi r^2 = 2$ when the Rayleigh formula leads to values larger than 2. The use of this highly simplified representation is especially recommended for particle size distributions in which the oscillatory behavior of the scattering cross section for $|\rho| \gg 1$ (cf. Section 4-2B) tends to become relatively unimportant.

Equations (4-2.5) and (4-2.5a) have been derived for macroscopic particles with complex index of refraction. They may be used for deduction of the formula for Rayleigh scattering from a homogeneous medium composed of spherical molecules, a relation which was first used by Rayleigh to explain the blue color of the clear sky, whereas particle scattering is responsible for the red color of the sunset. For a homogeneous medium composed of spherical gas molecules, the index of refraction is real and close to unity, i.e.,

$$N^2 - 1 \simeq N_1^2 - 1 \qquad \text{and} \qquad N^2 + 2 \simeq 3.$$

Furthermore, if $\mathcal{N}$ denotes the number of scattering centers per unit volume, then Rayleigh's results are obtained by writing

$$\mathcal{N} = \frac{1}{\frac{4}{3}\pi r^3},$$

where r is the radius previously used for the macroscopic particles. In this manner, the following relations are obtained for scattering from homogeneous spherical molecules (quantities referring to this special case are identified by the supplementary subscript m):

$$Q_{s,m} = \frac{8}{3}\frac{\pi^3}{\lambda^4}\frac{(N_1^2 - 1)^2}{\mathcal{N}^2}, \tag{4-2.6}$$

$$Q_{s,m}(\theta) = \frac{\pi^2}{2\lambda^4}\frac{(N_1^2 - 1)^2}{\mathcal{N}^2}(1 + \cos^2\theta), \tag{4-2.6a}$$

$$\kappa_{s,m} = \frac{2^{13/3}\pi^{8/3}}{3^{5/3}\lambda^4}\frac{(N_1^2 - 1)^2}{\mathcal{N}^{4/3}}, \tag{4-2.7}$$

and

$$\kappa_{s,m}(\theta) = \frac{2^{1/3}\pi^{5/3}}{3^{2/3}\lambda^4}\frac{(N_1^2 - 1)^2}{\mathcal{N}^{4/3}}(1 + \cos^2\theta). \tag{4-2.7a}$$

Typical values of $\mathcal{N} \times [Q_{s,m}(\theta = \pi/2)]$ for air constituents at $\lambda = 5000$ Å are of the order of 3×10^{-7} cm^{-1} for $\mathcal{N} = 10^{18}$ cm^{-3}.

As an illustration of scattering calculations on homogeneous gases, we may estimate the fraction of the incident intensity scattered at right angles with respect to the incident intensity, per unit volume of the scattering medium, into the solid angle $\Delta\theta$ (see Fig. 4-2.1). Consider an

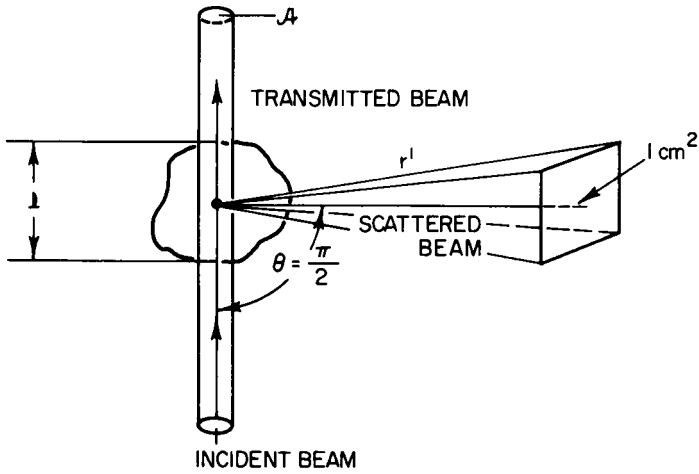

FIG. 4-2.1. Schematic diagram illustrating right-angle scattering from a homogeneous gas.

incident beam of cross-sectional area $\mathscr{A}$, which is scattered by gases contained in the geometric length l, into the solid angle $\Delta\theta = 1/(r')^2$, where $r' \gg l$. According to Eq. (4-2.6a), the fraction of the scattered intensity becomes

$$f(\theta = \pi/2) = Q_{s,m}(\theta = \pi/2)\mathscr{N} l\mathscr{A}\,\Delta\theta$$

or

$$\frac{f(\theta = \pi/2)\,(r')^2}{V} = \frac{\pi^2}{2\lambda^4}\frac{(N_1^2 - 1)^2}{\mathscr{N}} \equiv \mathscr{R} \tag{4-2.8}$$

where $V = l\mathscr{A}$ and the quantity appearing in Eq. (4-2.8) is sometimes called the "Rayleigh ratio," which represents physically the fraction of the incident beam scattered, per unit volume, per unit solid angle, under the specified conditions. The molar refractivity (with dimensions cm^3-$mole^{-1}$) is defined as

$$A = \frac{\mathscr{N}_A}{\mathscr{N}}\frac{N_1^2 - 1}{N_1^2 + 2},$$

where $\mathcal{N}_A$ represents the Avogadro number; it is known (see, for example, Born and Wolf,[3] pp. 88–89) that A is very nearly constant, whence it follows that the Rayleigh ratio $\mathcal{R}$ may be written in the form

$$\mathcal{R} = \frac{9\pi^2}{2\lambda^4} \frac{A^2}{(\mathcal{N}_A)^2} \mathcal{N} \tag{4-2.9}$$

for $N_1^2 + 2$ approximated by 3. Equation (4-2.9) shows that the fraction of the scattered intensity per unit volume, into the given solid angle, is directly proportional to the number of scattering centers. Numerical values for the molar refractivity are given, for example, in Born and Wolf[3] (see pp. 88–89), where procedures are also described for calculating A for gas mixtures from values known for the pure components, and for molecules from atomic refractivities. For pressures between about 1 and 176 atm, for sodium D light, $A \simeq 2.2$ cm^3-mole^{-1} and, for $\mathcal{N} = 10^{18}$ cm^{-3}, $\mathcal{R} \simeq 10^{-6}$ cm^{-3}-sterad^{-1}.

4-2B SCATTERING ACCORDING TO THE KIRCHHOFF-HUYGENS PRINCIPLE ($|\rho| \gg 1$). For $|\rho| \gg 1$, the asymptotic forms for a_n^r and b_n^r become, respectively,[2]

$$a_n^r \simeq i^n(\exp - i\rho) \frac{\mu_s(\sin x) - \mu_m N(\cos x)(\tan y)}{\mu_s - i\mu_m N(\tan y)} \qquad \text{for} \quad n \ll |\rho|, |N\rho|,$$

and

$$b_n^r \simeq -i^{n+1}(\exp - i\rho) \frac{\mu_s(\cos x)(\tan y) - \mu_m N(\sin x)}{\mu_s(\tan y) + i\mu_m N} \qquad \text{for} \quad n \ll |\rho|, |N\rho|,$$

where

$$x = \rho - \frac{n+1}{2}\pi, \qquad y = N\rho - \frac{n+1}{2}\pi.$$

Hence the coefficients a_n^r and b_n^r (where $a_{n+1}^r \simeq b_n^r$) are oscillating functions of ρ and n, which vary in absolute value between zero and unity for small changes in these parameters (cf. Figs. 4-1.1 to 4-1.4).

It is neither physically nor mathematically obvious that the use of the preceding relations in Eqs. (4-1.6) and (4-1.7) leads to the limiting expression $Q_t/\pi r^2 = 2$ (cf. Figs. 4-1.1 to 4-1.4). The factor 2, rather than unity, arises because the approximation of geometrical optics necessarily fails in the immediate vicinity of the particle boundary (see Born and Wolf,[3] pp. 659–660). In the limit $r \gg \lambda$, the intensity of radiation scattered in the forward direction may be several orders of magnitude larger than the intensity of radiation scattered in the backward direction. A restricted derivation of the Kirchhoff-Huygens limit from the Mie

theory is sketched in Appendix 4-1; the discussion given in the appendix will serve to emphasize the well-known fact that the complete Mie theory should only be used when other procedures are not available. For a conventional approach to the Kirchhoff-Huygens limit, we refer to Van de Hulst's derivation from diffraction theory.[5]

In conclusion, it appears appropriate to emphasize the relations that are applicable to macroscopic problems for which $|\rho| \gg 1$. For non-absorbing spheres,

$$Q_s/\pi r^2 = Q_t/\pi r^2 = 2, \qquad Q_a = 0;$$

on the other hand, for completely opaque spheres,

$$Q_a/\pi r^2 = 1.$$

Furthermore, since scattering occurs almost exclusively in the forward direction, the total attenuation of the incident beam is practically determined by the geometric cross section. For partially transparent spheres, the attenuation of beam intensity is also determined by the geometric cross section which must, however, now be multiplied by an appropriate transmissivity.

4-3 Emission and scattering of radiation from distributions of carbon particles

When the particles are separated by distances that are large compared to the wavelength of the incident radiation, then it is permissible to treat the scattering and emission centers as independent. Before discussing the results of representative numerical calculations, it appears appropriate to consider the proper formulation of the problem of radiant-energy emission and scattering from a distribution of small particles.

4-3A EMISSION AND SCATTERING OF RADIATION FROM A PARTICLE-SIZE DISTRIBUTION.[6] As for individual spherical particles, we define for particle-size distributions the total cross section Q_t as the sum of the absorption (Q_a) and scattering (Q_s) cross sections. The energy flux $dE_\nu(\theta, \varphi)$ through an element of surface dS, in a direction defined by the angles φ and θ (see Fig. 4-3.1), from the particles contained within the volume element dV, becomes

$$dE_\nu(\theta, \varphi) = \frac{B_\nu(T)\,[\mathcal{N}_p Q_a(\nu)\,dV]}{r^2}\,[\exp(-Q_t \mathcal{N}_p r)]\,dS\cos\theta, \qquad (4\text{-}3.1)$$

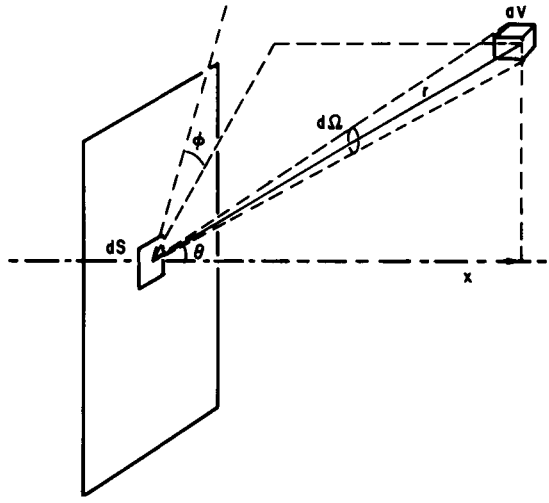

FIG. 4-3.1. Diagram showing the geometric arrangement used for the calculation of radiation through the surface dS and emitted from the volume dV; reproduced from Stull and Plass.[6]

where $B_\nu(T)$ denotes again the appropriate blackbody steradiancy and $\mathcal{N}_p$ is now the total number of particles per unit volume. The term $\exp(-Q_t\mathcal{N}_p r)$ measures the fraction of the emitted radiation which is neither scattered or absorbed. Since $dV = r^2\, d\Omega\, dr$, it follows that the total flux density, per unit solid angle and per unit surface area associated with emission in dV, becomes

$$[I_\nu(\theta, \varphi)]_e = \int_0^{x_{max}} \frac{dE_\nu(\theta, \varphi)}{d\Omega\, dS}$$

$$= B_\nu(T)\, \mathcal{N}_p Q_a(\nu) \int_0^{x_{max}} [\exp(-\mathcal{N}_p Q_t x \sec\theta)]\, dx, \qquad (4\text{-}3.2)$$

where we have assumed that the temperature is constant and x is measured in the direction normal to dS (i.e., $x = r\cos\theta$).

For a scattering medium, we must include also the radiant energy scattered into the volume element dV which reaches dS. The radiant energy entering dV from dV' is

$$B_\nu(T)\, Q_a(\nu)\, \mathcal{N}_p \frac{1}{(r')^2}\, d\Omega'\, dV' [\exp(-\mathcal{N}_p Q_t r')]$$

if $d\Omega'$ is the solid angle subtended by dV at dV' and r' is the geometric path length for a ray within $d\Omega'$ between dV' and dV; of this incident

radiant energy, the fraction $Q_s(\nu)\mathcal{N}_p\, dr'$ is scattered in dV if dr' is the geometric path length of the ray r' within dV. Hence, the rate at which radiant energy is emitted into dV, and then scattered in dV toward dS, becomes

$$[I_\nu(\theta, \varphi)]_{sc}\, d\Omega\, dS = B_\nu(T)\frac{\mathcal{N}_p Q_a(\nu)}{4\pi}\int_{V'}\frac{[\exp(-\mathcal{N}_p Q_t r')]}{(r')^2}\, dV' \times \frac{\mathcal{N}_p Q_s(\nu)}{r^2}[\exp(-\mathcal{N}_p Q_t r)]\, dV\, dS\cos\theta, \qquad (4\text{-}3.2a)$$

where the integral over V' extends over the entire distribution. In the derivation of Eq. (4-3.2a), we have evidently only included single scattering. From Eqs. (4-3.2) and (4-3.2a), it is apparent that the total steradiancy through dS becomes

$$\begin{aligned} I_\nu(\theta, \varphi) &= [I_\nu(\theta, \varphi)]_e + [I_\nu(\theta, \varphi)]_{sc} \\ &= B_\nu(T)\,\mathcal{N}_p Q_a(\nu)\int_0^{x_{max}}[\exp(-\mathcal{N}_p Q_t x\sec\theta)] \\ &\quad \times \left\{1 + [\mathcal{N}_p Q_s(\nu)/4\pi]\int_{V'}(r')^{-2}[\exp(-\mathcal{N}_p Q_t r')]\, dV'\right\} dx. \end{aligned} \qquad (4\text{-}3.3)$$

For multiple isotropic scattering, it may then be shown[6] that

$$\begin{aligned} I_\nu(\theta, \varphi) &= B_\nu(T)\,\mathcal{N}_p Q_a(\nu)\int_0^{x_{max}}[\exp(-\mathcal{N}_p Q_t x\sec\theta)] \\ &\quad \times \left\{1 + \left[[\mathcal{N}_p Q_s(\nu)/4\pi]\int_{V'}(r')^{-2}[\exp(-\mathcal{N}_p Q_t r')]\right]\right. \\ &\quad \left. \times \left\{1 + [\mathcal{N}_p Q_s(\nu)/4\pi]\int_{V''}(r'')^{-2}[\exp -\mathcal{N}_p Q_t r'']\{1 + \cdots\}\, dV''\right\} dV'\right\} dx. \end{aligned} \qquad (4\text{-}3.3a)$$

The treatment of multiple, isotropic scattering is valid for spherical particles, and derivation of the preceding relations involves the assumption that all absorption and scattering cross sections are equal. If the number of particles in the size range between r and $r + dr$ is $\mathcal{N}(r)\, dr$, then a repetition of the derivation of Eqs. (4-3.1) to (4-3.3a) shows that these relations still hold if each cross section is replaced by a suitable average value, viz.

$$\langle Q(\nu)\rangle_{av} = \frac{1}{\mathcal{N}_p}\int_0^\infty Q(\nu, r)\mathcal{N}(r)\, dr. \qquad (4\text{-}3.4)$$

For sufficiently small values of Q_s/Q_t, the scattering terms may be neglected in Eqs. (4-3.3) and (4-3.3a) and the total steradiancy becomes equal to the emission term. After integration, we find then that

$$[I_\nu(\theta, \varphi)]_e = B_\nu(T)\,[Q_a(\nu)/Q_t(\nu)] \cos\theta \times [1 - \exp(-Q_t L)],$$
$$L = \mathcal{N}_p x_{max} \sec\theta. \tag{4-3.5}$$

4-3B APPLICATION TO CARBON PARTICLES. For carbon particles, over most of the size ranges considered by Stull and Plass,[6] the effect of scattering was unimportant and Eq. (4-3.4) constituted an adequate

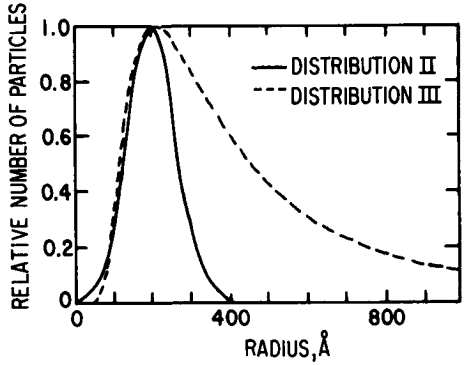

FIG. 4-3.2. Two particle-size distributions used for the calculation of the emissivity of carbon particles; reproduced from Stull and Plass.[6] Distribution II: $\mathcal{N}(r)\,dr = (\mathcal{N}_p/159.52)\{\exp[-(r - 200)/90]^2\}\,dr$; distribution III: $\mathcal{N}(r)\,dr = 4.75 \times 10^5\,\mathcal{N}_p r^{-3} \times [\exp(-640/r)]\,dr$ for $50 \leqslant r$ (Å) $\leqslant 1000$ and $\mathcal{N}(r)\,dr = 0$ for other values of r.

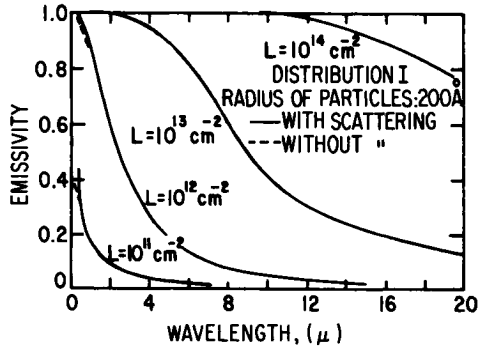

FIG. 4-3.3. Emissivity as a function of wavelength for carbon particles of 200-Å radius. The results are shown when the scattering terms are included in the calculations and when they are omitted; reproduced from Stull and Plass.[6] Distribution I: particles of uniform radius.

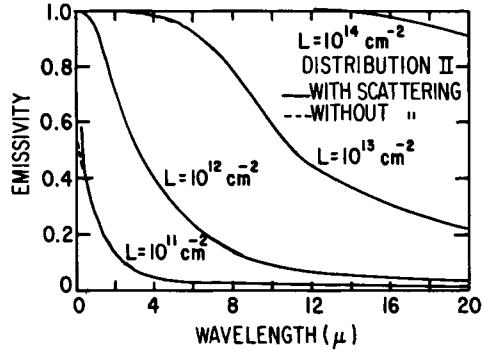

FIG. 4-3.4. Emissivity as a function of wavelength for particle-size distribution II; reproduced from Stull and Plass.[6]

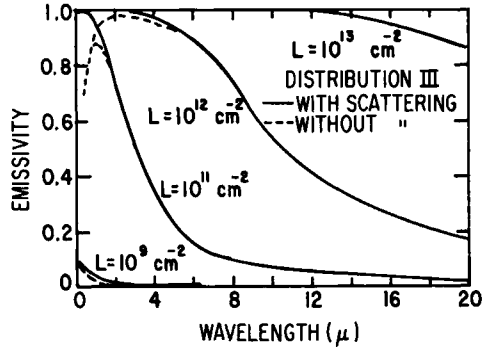

FIG. 4-3.5. Emissivity as a function of wavelength for particle-size distribution III; reproduced from Stull and Plass.[6]

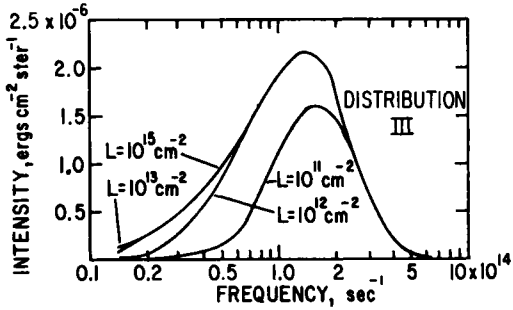

FIG. 4-3.6. Emitted intensity at 2250°K as a function of wavelength for particle-size distribution III; reproduced from Stull and Plass.[6]

approximation. The method for including scattering when it is not negligible is also described by Stull and Plass.[6] These authors considered the size distributions sketched in Fig. 4-3.2 and obtained many numerical results, some of which are reproduced in Figs. 4-3.3 to 4-3.5 and all of which refer to the case $\theta = 0$. Reference to Figs. 4-3.3 to 4-3.5 shows that the contributions of scattering are negligibly small, except at the smallest wavelengths. Furthermore, the presence of larger particles in the distributions II and III produces a noticeable increase in emissivity at long wavelengths. The intensity of radiation, which is actually emitted, is shown in Fig. 4-3.6 for distribution III at 2250°K for various values of L; at $L = 10^{15}$ cm^{-2}, the intensity curve corresponds to that of a blackbody. The results of Stull and Plass may be summarized by the statement that, for $L \leqslant 10^{9}$ cm^{-2}, the emission between 0.4 and 20 μ is very weak; on the other hand, for $L \geqslant 10^{16}$ cm^{-2}, it approaches blackbody emission. For $r = 200$ Å, the specified limits for low and near-blackbody emission should be modified to 10^{11} and 10^{14} cm^{-2}, respectively.

4-4 Scattering and emission from distributions of alumina and magnesia particles[8]

For particles of alumina and magnesia, it turns out that $Q_s \gg Q_a$. In this limit, the scattering problem reduces to the neutron albedo problem, which has been solved exactly.[9] In particular, for a semiinfinite homogeneous slab of material, it is found that the spectral emissivity becomes

$$\epsilon_\nu = q[Q_a(\nu)/Q_s(\nu)]^{1/2}, \qquad Q_s(\nu)/Q_a(\nu) \gg 1, \tag{4-4.1}$$

where $q = 2.91$ for the direction perpendicular to the surface of the slab and $q = 2.31$ for the hemispherical emissivity. The functional (square-root) form of Eq. (4-4.1) may be understood in terms of a random-walk model. In the limiting case $Q_a x_{max} \mathcal{N}_p \ll 1$, $Q_s x_{max} \mathcal{N}_p \ll 1$, the hemispherical emissivity becomes independent of the presence of the scatterers, although the angular distribution is affected by scattering.[8]

For a medium of finite thickness with anisotropic scattering, the problem of radiant-energy emission becomes extremely complex.[10]

Bauer and Carlson[8] have performed Mie scattering calculations for particle-size distributions of alumina and magnesia fitting the two-parameter relation

$$\mathcal{N}(r)\, dr = \frac{a^{b+1}}{b!}\, r^b\, [\exp(-ar)]\, dr$$

for $a(\mu^{-1}) = 2.5$, 3.0, and 0.8 and $b = 0.5$, 0.6, and 0.6, respectively. In particular, these authors have evaluated the differential scattering cross section $i_{av}(\theta)$ as a function of θ at different wavelengths. The differential scattering cross section $i_{av}(\theta)$ may be used to estimate the intensity contributed by one particle of cross section Q_s, per steradian, by using the relation

$$I_\nu(\theta) = \frac{I'_\nu Q_s i_{av}(\theta)}{2\pi \int_0^\infty i_{av}(\theta) \sin\theta \, d\theta}, \tag{4-4.2}$$

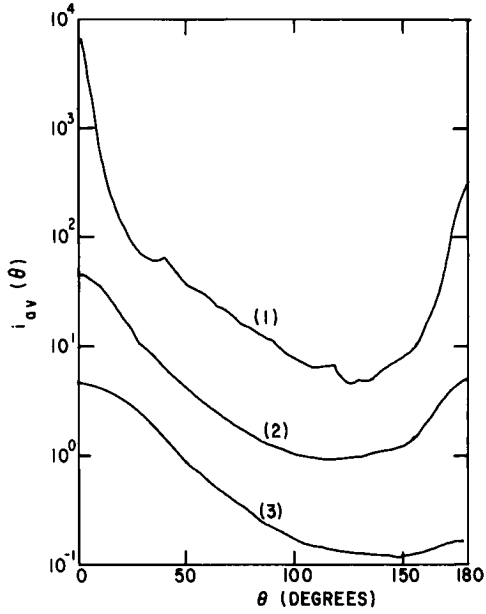

FIG. 4-4.1. Differential scattering cross section for alumina particles with $b = 0.6$, $a = 3.0\ \mu^{-1}$. (1) $\lambda = 0.5\ \mu$; $N_2 = 10^{-3}$. (2) $\lambda = 2.0\ \mu$; $N_2 = 10^{-5}$ or 10^{-6}. (3) $\lambda = 4.0\ \mu$; $N_2 = 10^{-5}$. (Here N_2 denotes again the imaginary part of the refractive index, which is related to the linear absorption coefficient k_λ by the expression $k_\lambda = 4\pi N_2/\lambda$.) Reproduced from Bauer and Carlson.[8]

where I'_ν is the incident radiancy of unpolarized radiation. Typical curves are reproduced in Fig. 4-4.1. In general, the use of particle-size distributions makes for more nearly isotropic scattering.

The temperature dependence of the Mie scattering and absorption cross sections is discussed in a recent paper by Plass.[7a]

Appendix 4-1

Scattering by nonabsorbing spheres for $N \gg 1$ or $N \ll 1$*

The correct relations for the total, scattering, and absorption cross sections, subject to the condition that $\rho \gg 1$, may be derived from the general expressions obtained by Mie according to the following arguments.

The total cross section is given by Eq. (4-1.8). Using the relations

$$\sigma_n(\rho) \equiv \frac{d}{d\rho} \ln[\rho j_n(\rho)] = \frac{j_{n-1}(\rho)}{j_n(\rho)} - \frac{n}{\rho} \tag{A-4.1}$$

and

$$\psi_n(\rho) \equiv \frac{d}{d\rho} \ln[\rho h_n^{(1)}(\rho)] = \frac{h_{n-1}^{(1)}(\rho)}{h_n^{(1)}(\rho)} - \frac{n}{\rho}, \tag{A-4.2}$$

where ρ is real for a nonabsorbing sphere, we find that Eqs. (4-1.3) and (4-1.4) become (for $\mu_s = \mu_m$), respectively,

$$a_n^r \equiv a_n = -\frac{j_n(\rho)}{h_n^{(1)}(\rho)} \frac{[\sigma_n(\rho) - N\sigma_n(N\rho)]}{[\psi_n(\rho) - N\sigma_n(N\rho)]} \tag{A-4.3}$$

and

$$b_n^r \equiv b_n = -\frac{j_n(\rho)}{h_n^{(1)}(\rho)} \frac{[\sigma_n(N\rho) - N\sigma_n(\rho)]}{[\sigma_n(N\rho) - N\psi_n(\rho)]}. \tag{A-4.4}$$

In general,

$$\frac{\sigma_n(\xi)}{\psi_n(\xi)} = \frac{[J_{n-1/2}(\xi)/J_{n+1/2}(\xi)] - (n/\xi)}{[H_{n-1/2}^{(1)}(\xi)/H_{n+1/2}^{(1)}(\xi)] - (n/\xi)}, \tag{A-4.5}$$

whence it follows that

$$\frac{\sigma_n(\xi)}{\psi_n(\xi)} \to 1 \qquad \text{as} \quad \frac{n}{\xi} \to \infty, \tag{A-4.5a}$$

$$\frac{\sigma_n(\xi)}{\psi_n(\xi)} \to \frac{J_{n-1/2}(\xi)}{H_{n-1/2}^{(1)}(\xi)} \frac{H_{n+1/2}^{(1)}(\xi)}{J_{n+1/2}(\xi)} \qquad \text{as} \quad \frac{n}{\xi} \to 0, \tag{A-4.5b}$$

* The material contained in this appendix is taken from unpublished work by Penner and Sharma.[11]

and

$$\frac{\sigma_n(\xi)}{\psi_n(\xi)} \to 1 \qquad \text{for large } n \text{ and } \xi \text{ as } \frac{n}{\xi} \to 1. \tag{A-4.5c}$$

The last limiting expression is best derived by using known asymptotic expansions for large n of the Bessel and Hankel functions.[12] Thus, for $a < 1$, $a = 1/\cosh \alpha$:

$$H_n^{(1)}(an) \simeq -i\left(\frac{2}{\pi n \tanh \alpha}\right)^{1/2} \exp\left[n(\alpha - \tanh \alpha)\right],$$

$$H_n^{(2)}(an) \simeq i\left(\frac{2}{\pi n \tanh \alpha}\right)^{1/2} \exp\left[n(\alpha - \tanh \alpha)\right],$$

$$J_n(an) \simeq \frac{2}{(2\pi n \tanh \alpha)^{1/2}} \exp\left[n(\tanh \alpha - \alpha)\right]; \tag{A-4.6}$$

for $a = 1$:

$$H_n^{(1)}(n) \simeq -\frac{1}{3\pi}\left[\Gamma\left(\frac{1}{3}\right)\right]\left\{\left[\exp\left(\frac{5\pi i}{6}\right)\right] + i\right\}\left(\frac{6}{n}\right)^{1/3},$$

$$H_n^{(2)}(n) \simeq -\frac{1}{3\pi}\left[\Gamma\left(\frac{1}{3}\right)\right]\left\{\left[\exp\left(-\frac{5\pi i}{6}\right)\right] - i\right\}\left(\frac{6}{n}\right)^{1/3},$$

$$J_n(n) \simeq -\frac{1}{3\pi}\left[\Gamma\left(\frac{1}{3}\right)\right]\left(\cos\frac{5\pi}{6}\right)\left(\frac{6}{n}\right)^{1/3}; \tag{A-4.7}$$

for $a > 1$, $a = 1/\cos \alpha$:

$$H_n^{(1)}(an) \simeq -\left(\exp\frac{3\pi i}{4}\right)\left(\frac{2}{\pi n \tan \alpha}\right)^{1/2} \exp\left[in(\tan \alpha - \alpha)\right],$$

$$H_n^{(2)}(an) \simeq -\left(\exp -\frac{3\pi i}{4}\right)\left(\frac{2}{\pi n \tan \alpha}\right)^{1/2} \exp\left[-in(\tan \alpha - \alpha)\right],$$

$$J_n(an) \simeq -\left(\frac{2}{\pi n \tan \alpha}\right)^{1/2} \cos\left[n(\tan \alpha - \alpha) + \left(\frac{3\pi}{4}\right)\right]$$

$$\simeq \left(\frac{2}{\pi an}\right)^{1/2} \cos\left[an - \frac{(2n+1)}{4}\pi\right] \qquad \text{for very large } an. \tag{A-4.8}$$

The next-higher-order terms in Eqs. (A-4.6) to (A-4.8) are of magnitude $n^{-1/4}$ or $n^{-1/5}$ compared to the first-order terms. We use asymptotic expansions for large n because we wish to study the contribution of the different terms in the infinite series as n becomes larger and larger. Equation (A-4.5c) follows most obviously by using Eq. (A-4.7) and noting that

$$J_{n-1/2}(n) \simeq J_{n-1/2}(n - \tfrac{1}{2}), \qquad J_{n+1/2}(n) \simeq J_{n+1/2}(n + \tfrac{1}{2}),$$

$$H_{n-1/2}^{(1)}(n) \simeq H_{n-1/2}^{(1)}(n - \tfrac{1}{2}), \qquad \text{and} \qquad H_{n+1/2}^{(1)}(n) \simeq H_{n+1/2}^{(1)}(n + \tfrac{1}{2}),$$

where the indicated approximations introduce higher-order corrections.

In view of Eqs. (A-4.5a) to (A-4.5c), we find from Eqs. (A-4.3) and (A-4.4) that

$$a_n^r, b_n^r \simeq -\frac{j_n(\rho)}{h_n^{(1)}(\rho)} \quad \text{or} \quad -\frac{j_{n-1}(\rho)}{h_{n-1}^{(1)}(\rho)} \tag{A-4.9}$$

for $N \gg 1$ and for $N \ll 1$; furthermore, for sufficiently large values of n, the differences in the ratios appearing in Eq. (A-4.9) are unimportant. Hence the problem of computing the total cross section has been reduced to the calculation of

$$Q_t = \frac{2\pi r^2}{\rho^2} \sum_n (2n+1)\, 2 \operatorname{Re}\left(\frac{j_n(\rho)}{h_n^{(1)}(\rho)}\right). \tag{A-4.10}$$

It is now convenient to note that

$$\operatorname{Re}\left(\frac{j_n(\rho)}{h_n^{(1)}(\rho)}\right) = \frac{J_{n+1/2}^2(\rho)}{J_{n+1/2}^2(\rho) + N_{n+1/2}^2(\rho)}, \tag{A-4.11}$$

$$\operatorname{Re}\left(\frac{j_n(\rho)}{h_n^{(1)}(\rho)}\right) = \frac{\pi\rho}{2} J_{n+1/2}^2(\rho) \quad \text{for} \quad \frac{\rho}{n} = a > 1, \tag{A-4.11a}$$

$$\operatorname{Re}\left(\frac{j_n(\rho)}{h_n^{(1)}(\rho)}\right) \text{ does not contribute appreciably for } \frac{\rho}{n} = a = 1, \tag{A-4.11b}$$

and

$$\operatorname{Re}\left(\frac{j_n(\rho)}{h_n^{(1)}(\rho)}\right) \to 0 \quad \text{if } n \text{ is sufficiently large for } \frac{\rho}{n} = a < 1. \tag{A-4.11c}$$

Furthermore, for large values of ρ and $a > 1$,

$$\begin{aligned} \frac{\pi\rho}{2} J_{n+1/2}^2(\rho) &\simeq \left\{\cos\left[\rho - \frac{(n+1)}{2}\pi\right]\right\}^2 \\ &= \left(\sin^2\frac{n\pi}{2}\right)(\cos^2\rho) + \left(\cos^2\frac{n\pi}{2}\right)(\sin^2\rho) \\ &\quad - 2(\sin\rho)(\cos\rho)\left(\sin\frac{n\pi}{2}\right)\left(\cos\frac{n\pi}{2}\right) \end{aligned}$$

or, since n is an integer,

$$\frac{\pi\rho}{2} J_{n+1/2}^2(\rho) = \left(\sin^2\frac{n\pi}{2}\right)\left(\cos^2\rho\right) + \left(\cos^2\frac{n\pi}{2}\right)(\sin^2\rho) \to \frac{1}{2} \text{ on the average.}$$

The use of the preceding relation in the expression

$$\sum_n (2n + 1)\, 2 \operatorname{Re}\left[\frac{j_n(\rho)}{h_n^{(1)}(\rho)}\right]$$

shows that

$$\sum_{n=1}^{\infty} (2n + 1)\, 2 \operatorname{Re}\left[\frac{j_n(\rho)}{h_n^{(1)}(\rho)}\right] = \sum_{n=1}^{\rho} (2n + 1)$$

$$\simeq \int_1^{\rho} (2n + 1)\, dn \simeq \rho^2 \qquad \text{(A-4.12)}$$

for sufficiently large values of ρ. Introduction of Eq. (A-4.12) into Eq. (A-4.10) leads to the result

$$\frac{Q_t}{\pi r^2} = 2 \qquad \text{for large } \rho.$$

A completely equivalent proof may be developed showing that

$$\frac{Q_s}{\pi r^2} = 2 \quad \text{and} \quad \frac{Q_a}{\pi r^2} = 0 \qquad \text{for large real values of } \rho,$$

i.e., for nonabsorbing spheres.

References

1. G. Mie, *Ann. Physik* [4] **25**, 377 (1908).
2. J. A. Stratton, "Electromagnetic Theory," pp. 563–573. McGraw-Hill, New York, 1941.
3. M. Born and E. Wolf, "Principles of Optics," Chapter XIII. Macmillan, New York, 1964.
4. R. M. Goody, "Atmospheric Radiation I. Theoretical Basis," Chapter 7. Oxford Univ. Press (Clarendon), London and New York, 1964.
5. H. C. Van de Hulst, "Light Scattering by Small Particles." Wiley, New York, 1957; see also W. M. Irvine, *J. Opt. Soc. Am.* **55**, 16 (1965).

5a. G. N. Plass, *Appl. Opt.* **5**, 279 (1966); G. W. Kattawar and G. N. Plass, *ibid.* **6**, 1377 and 1543 (1967).

6. V. R. Stull and G. N. Plass, *J. Opt. Soc. Am.* **50**, 121 (1960).
7. G. N. Plass, *Appl. Opt.* **3**, 867 (1964).

7a. G. N. Plass, *Appl. Opt.* **4**, 1616 (1965).

8. E. Bauer and D. J. Carlson, *J. Quant. Spectry. & Radiative Transfer* **4**, 363 (1964).
9. O. Halpern, R. Lueneburg, and O. Clark, *Phys. Rev.* **53**, 173 (1938).
10. L. M. Romanova, *Opt. Spectry. (USSR) (English Transl.)* **13**, 238 and 463 (1962); **14**, 135 (1963).
11. S. S. Penner and O. P. Sharma, unpublished work (1965).
12. R. Courant and D. Hilbert, "Methoden der Mathematischen Physik," Vol. 1, pp. 456–460. Springer, Berlin, 1931.